Report Internship

In-plane vibration control of a cable driven parallel robot

FINAL VERSION
DC 2017.054

Author:	D.T. Fresen (David)	0722462
Supervisor:	prof. dr. H. Nijmeijer	
Coaches:	prof. dr. A. Khajepour (UW)	
	dr. ir. H. Jamshidifar (UW)	

Eindhoven University of Technology
Department of Mechanical Engineering
Section Dynamics and Control

In collaboration with the University of Waterloo, Ontario, Canada

April 19, 2017

Abstract

Cable driven parallel robots have a great potential in applications where high accelerations and low costs are required. However due to the low stiffness characteristic of cable robots, vibrations tend to occur which quickly limit the performance. Therefore, in order to make cable driven parallel robots a viable application in industry, an active vibration controller is required.

In this research a cable driven parallel robot has been studied and a simple but effective vibration controller has been designed and tested. Using various system identification techniques, the characteristics of the system based on the position of the end-effector have been determined.

Based on these measurements, a decoupled PD controller using adaptive gains has been proposed that attenuates vibrations of the end-effector in both y- and θ-direction. Experimental results of the closed loop performance of the system validates the good vibration control capabilities of the proposed controller.

Contents

1 | Introduction

1.1 Background and motivation

In recent years there is an ever increasing demand for high throughput automated warehousing solutions. The use of a cable driven parallel robot (CDPR) is a relatively new concept which has not been implemented in large scale applications as of yet. Cable driven manipulators have a lot of advantages over traditional rigid link manipulators. The dynamic system can be designed with very low mass, since the (heavy) motors are statically attached to the world and cables have a much lower mass compared to alternative rigid links. This simple and lightweight design allows for high accelerations, large work spans and low setup and maintenance costs.

Because of the distinct advantages mentioned above, cable driven manipulators have gained a lot of interest from robotic researchers in recent years [1] [2]. A good industrial example is the DeltaBot, a cable based robot which is capable of performing 120 pick and place operations per minute [3]. Another example that shows the potential of cable driven manipulators is the FALCON robot which is able to reach a velocity of 14 m/s with accelerations of 40 g [4].

Another big advantage is the large workspace cable driven manipulators can occupy, due to the fact that the cables can be compactly coiled. The Arecibo radio telescope for example uses a CDPR with a span of over 300 metres to carry its 900 ton receiving platform 150 m in the air [5]. Since cables are readily available and don't have to be specifically designed and manufactured like traditional rigid links, they can be easily replaced or reconfigured. This results in overall lower costs as well as easier maintenance compared to traditional manipulator designs.

A challenge regarding the use of cables to move a manipulator is the fact that cables can only exert a unidirectional force. This means that the cables must be held under tension at all times. This complicates the task of controlling CDPRs since additional requirements have to be taken into account to ensure that cable tension is always maintained. Another disadvantage of CDPRs is the elastic nature of cables which result in low manipulator stiffness. Due to this low stiffness, end-effector vibrations pose a real limitation on the performance of the system. These vibrations have to be limited before CDPRs can be used on a large scale as warehousing solutions.

1.2   Objective

The objective of this research is to develop and implement an active vibration controller for a CDPR which is capable of attenuating undesired end-effector vibrations in the three in-plane degrees of freedom (DOF). Previous studies have been done regarding this subject where a complete dynamical model is available which takes all individual cables into account [10] [11]. The challenge of this research is to investigate whether the design of a vibration controller is possible using a more general and simplified 3 DOF mass-spring-damper model instead of a complex and detailed model of the system.

1.3   Outline of the report

Chapter 2 provides a description of the system. A model of this system is presented and the stiffness and vibration characteristics are found using different system identification methods.

In Chapter 3, the in-plane vibration control is elaborated. The control strategy is explained and a comparison is made between a decoupled PD approach and a LQR approach. Both methods are simulated to verify the performance in terms of vibration attenuation. Also the state estimation is explained in this chapter.

Chapter 4 presents the experimental results when the PD controller is implemented on the real system. Also the method for tuning the PD controller is explained.

Finally, Chapter 5 contains concluding remarks regarding the results obtained in this project and lists recommendations and suggestions for future work.

2 | System model and identification

In this chapter the system which is regarded for this research is described. A model and corresponding equations of motion for this system are derived. Finally, various system identification techniques are used to experimentally determine the stiffness and vibration characteristics for this system.

2.1 System description

The system for which a vibration controller will be designed consists of a moving platform (MP) suspended by a total of 12 cables. The length of these cables can be controlled using 4 different motors such that the MP can be positioned anywhere in the plane. The motors on the top left and top right each control the length of a bundle of four cables simultaneously. The bottom left and right motors both control two cables simultaneously. An approximate SolidWorks representation of the system is shown in Figure 2.2, with some specifications given in Table 2.1. A detailed SolidWorks representation of the MP is shown in Figure 2.1. The two pendula attached to the bottom of the MP are designed to attenuate the out of plane vibrations. However this research only considers in-plane vibrations, so these pendula are not used for this purpose.
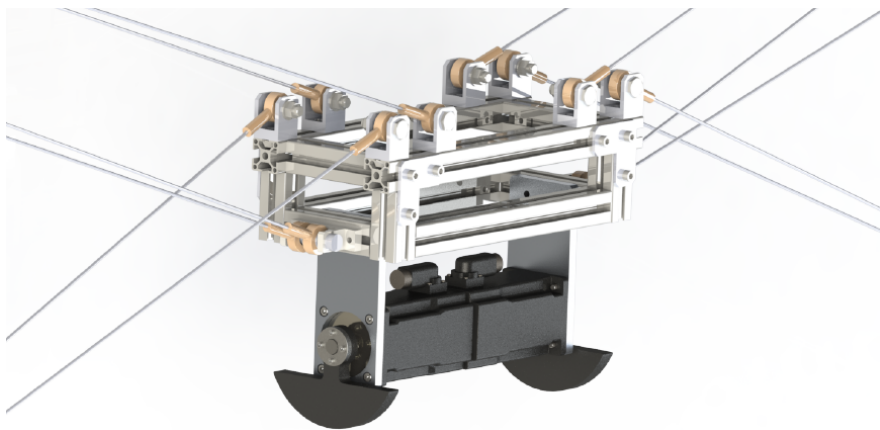

Figure 2.1: Detailed SolidWorks representation of the MP

An inertial measurement unit (IMU) is attached to the MP to measure the lateral accelerations in x, y and z as well as the three rotational velocities around these axes. The MP can be homed

within a couple millimetres of its homing position using a low resolution camera.

The bottom cables are equipped with force sensors which makes force control possible. Linear springs have been added to have more control of the force exerted by the cables on the MP. If the springs were to be removed a slight elongation would immediately result in a high reaction force. The springs also prevent cable slackness, which is a danger for CDPRs.
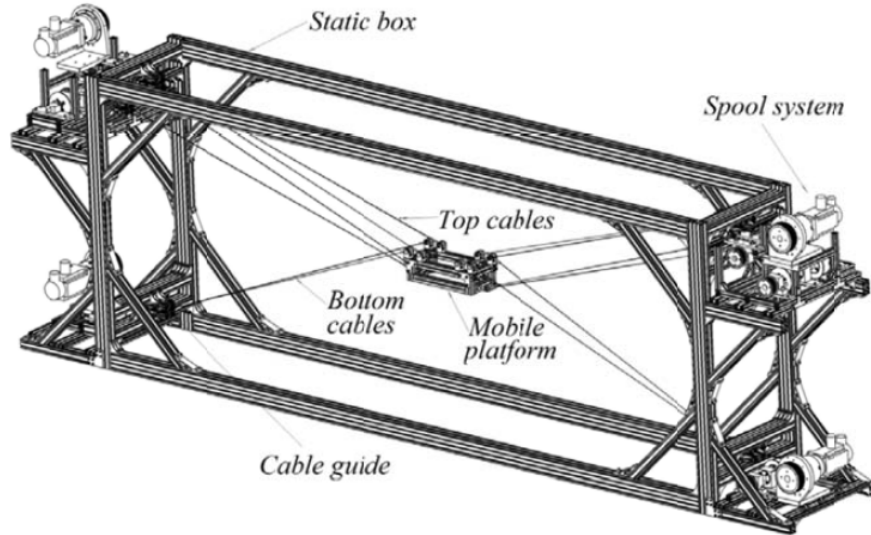

Figure 2.2: SolidWorks representation of the system

Table 2.1: Specifications of the system

Parameter	Value	Unit
a	1	m
b	3	m
h	0.07	m
w	0.21	m
m_p	12.2	kg
I_z	0.22	kg mˆ2

2.1.1 System model

The cables of a CDPR can be modelled with different levels of detail. In the most simple case the cables are assumed to be massless straight line segments with no elongation. For relatively simple and small scale cases this assumption has proven to work well [6] [7]. For large scale applications, such as the telescope application refered to in [5], a more detailed model is needed, one that takes

cable mass and cable sagging into account. In order to investigate the stiffness and vibration characteristics, cable elongation has to be taken into account. This way, the cables can be represented as a massless linear springs [8] [9].

The system when the MP is positioned at a stationary point in the workspace is represented as a decoupled, three degrees of freedom model as shown in Figure 2.3. This model represents the vibrational behaviour of the MP suspended by the 12 cables shown in Figure 2.2 when the MP is at a stationary position. Here k_i and c_i, $i \in x, y, \theta$ are the equivalent stiffness and damping values as a result of the stiffness and damping of all 12 individual cables combined. The equations of motion for this system can be written as three simple equations describing three separate mass-spring-damper systems in x-, y- and θ-direction.

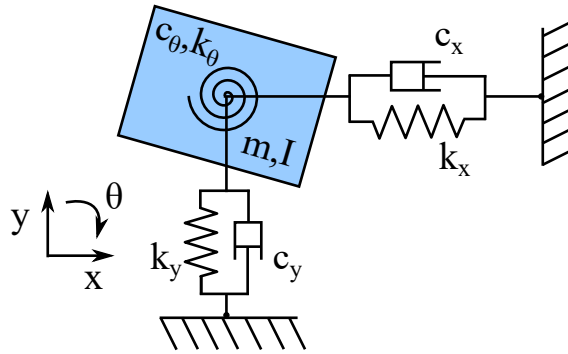Figure 2.3: Decoupled model in 3 degrees of freedom

The unforced system of equations of motion therefore becomes:

$$m\ddot{x} + c_x\dot{x} + k_x x = 0$$
$$m\ddot{y} + c_y\dot{y} + k_y y = 0 \qquad (2.1)$$
$$I\ddot{\theta} + c_\theta\dot{\theta} + k_\theta\theta = 0$$

The system properties in terms of stiffness and damping depend on the position of the MP in the workspace. The lengths of the various cables suspending the platform change according to the geometry of the system. Since a longer cable has a lower stiffness and damping coefficient, the overall stiffness and damping properties of the system change depending on the position of the platform.

Additionally, the tension of the bottom cables influences the stiffness of the whole system. However it has been shown that for the in-plane degrees of freedom which are considered in this research, the stiffness and damping properties are primarily determined by the configuration of the upper cables [11]. Therefore the assumption has been made that the bottom cables have a constant tension of 80 N and the equivalent stiffness and damping have been determined based on that.

With this position dependency included, the equations of motion become:

$$M \begin{bmatrix} \ddot{x} \\ \ddot{y} \\ \ddot{\theta} \end{bmatrix} + C(x,y) \begin{bmatrix} \dot{x} \\ \dot{y} \\ \dot{\theta} \end{bmatrix} + K(x,y) \begin{bmatrix} x \\ y \\ \theta \end{bmatrix} = \underline{0} \tag{2.2}$$

Where matrices M, K and C are all diagonal. Here K and C are unknown, position dependant and will be determined experimentally. Both a free vibration analysis and a forced vibration analysis has been done to identify the system and to find appropriate values for the stiffness matrix K and the damping matrix C for various points in the workspace.

Similarly the uncontrolled system can be written in standard state space form:

$$\dot{X} = A(x,y)X$$

Where the state X is defined as:

$$X = \begin{bmatrix} x & y & \theta & \dot{x} & \dot{y} & \dot{\theta} \end{bmatrix}^T \tag{2.3}$$

And the system matrix $A(x,y)$ is defined as:

$$\begin{aligned}
A(x,y) &= \begin{bmatrix} O_{3x3} & I_{3x3} \\ M^{-1}K(x,y) & M^{-1}C(x,y) \end{bmatrix} \\
&= \begin{bmatrix}
0 & 0 & 0 & 1 & 0 & 0 \\
0 & 0 & 0 & 0 & 1 & 0 \\
0 & 0 & 0 & 0 & 0 & 1 \\
-k_x/m & 0 & 0 & -c_x/m & 0 & 0 \\
0 & -k_y/m & 0 & 0 & -c_y/m & 0 \\
0 & 0 & -k_\theta/I & 0 & 0 & -c_\theta/I
\end{bmatrix}
\end{aligned} \tag{2.4}$$

Here k_i and c_i, $i \in x, y, \theta$ are the stiffness and damping constants in x-, y- and θ-direction respectively, depend on the MP position (x,y) and are defined as explained above.

2.2 Free vibration analysis

The free vibration response of the system has been analyzed in the three in-plane DOF x, y and θ separately by exciting the system using a hammer impulse in those directions. Due to practical

limitations, excitation purely in one direction is not possible. For example a pure y-excitation is not possible because the robot cannot be hit in the middle at the top or bottom, because that would damage fragile parts of the system. Instead it was excited downward at a corner point, which result in both a y- and θ-excitation as well as an out-plane motion simultaneously. However this does not restrict the ability to investigate the free vibration response in one direction, since the lateral acceleration in x- and y-direction and the angular velocity around z can be measured separately using the body fixed Inertial Measurement Unit (IMU).

The vibration response at position (x,y) = (0,0) in three DOF due to hammer excitation is shown as the blue line in Figure 2.4. The general solution of a linear free vibrating single DOF system, as derived in Appendix 5.2, can be written as:

$$x(t) = c_1 e^{-at} sin(bt + c_2) \tag{2.5}$$

Here, $a = \eta\omega_n$, $b = \omega_d = \omega_n\sqrt{\eta^2 - 1}$ and c_1 and c_2 are constants which depend on the initial conditions. Using (2.5) an optimal fit in the least square sense has been made through the measurement data. For this, the MATLAB function `lsqcurvefit` has been used which minimizes the summed square residuals. Here the summed square of residuals is given by

$$S = \sum_{i=1}^{n} (y_i - \hat{y}_i)^2$$

where n is the number of data points, y_i is the observed response value and $\hat{y}_i$ is the fitted response value. Now constants a, b, c_1 and c_2 are determined from the resulting fit which can be used to find the desired damping constant η and natural frequency ω_n.

Since acceleration data is measured and not displacement, (2.5) has to be differentiated twice. However by doing so, only the constants c_1 and c_2 change, while the values a and b which are used to determine the stiffness and damping matrix remain unchanged. Also from the measurement data it is clear that the real system cannot be regarded as a simple linear one DOF system, since multiple eigenfrequencies are present in all directions.

In order to get a better fit and therefore a better understanding of all the frequencies present in the signal, additional terms are added to the general solution (2.5). This means that for y and θ a solution of the form: $x(t) = c_1 e^{-at} sin(bt + c_2) + c_3 e^{-dt} sin(et + c_4)$ is used and for x a third term is added.

The results of the measured and fitted vibration response including the obtained natural frequencies f_n in Hz is shown in Figure 2.4.
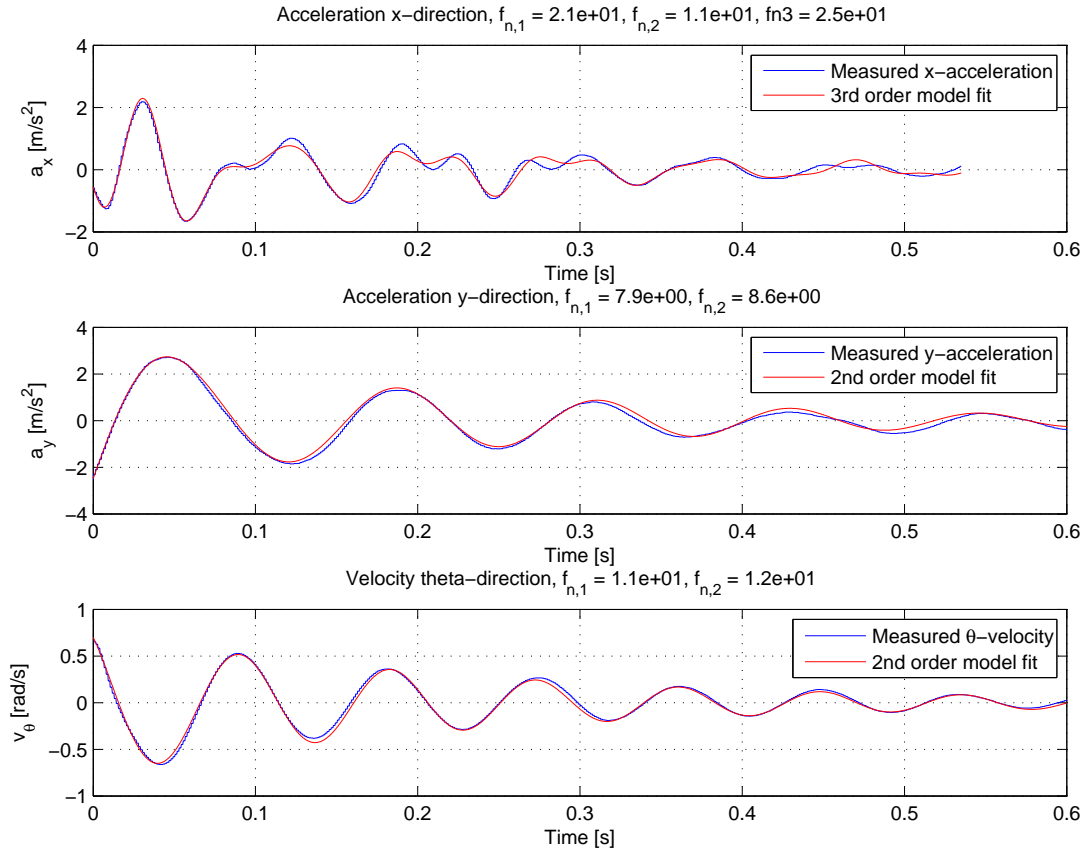
Figure 2.4: Free vibration response measurements and estimation fit

From the results obtained above and shown in Figure 2.4 it is clear that looking only at the vibration response does not give a clear indication of the dominant frequency present in the signals. Another way to determine the frequencies present in a signal is to look at the Power Spectral Density (PSD) plot using the Fast Fourier Transform. This plot indicates which frequencies are present in the signal and to what extend. The PSD plot of the three DOF in shown in Figure 2.5.

It can be seen that the eigenfrequencies obtained in both methods match well. In y-direction the PSD shows a clear peak at around 8.5 Hz, while in θ-direction a main peak at around 11.5 Hz can be identified. In x-direction the main eigenfrequency lays at around 20 Hz.
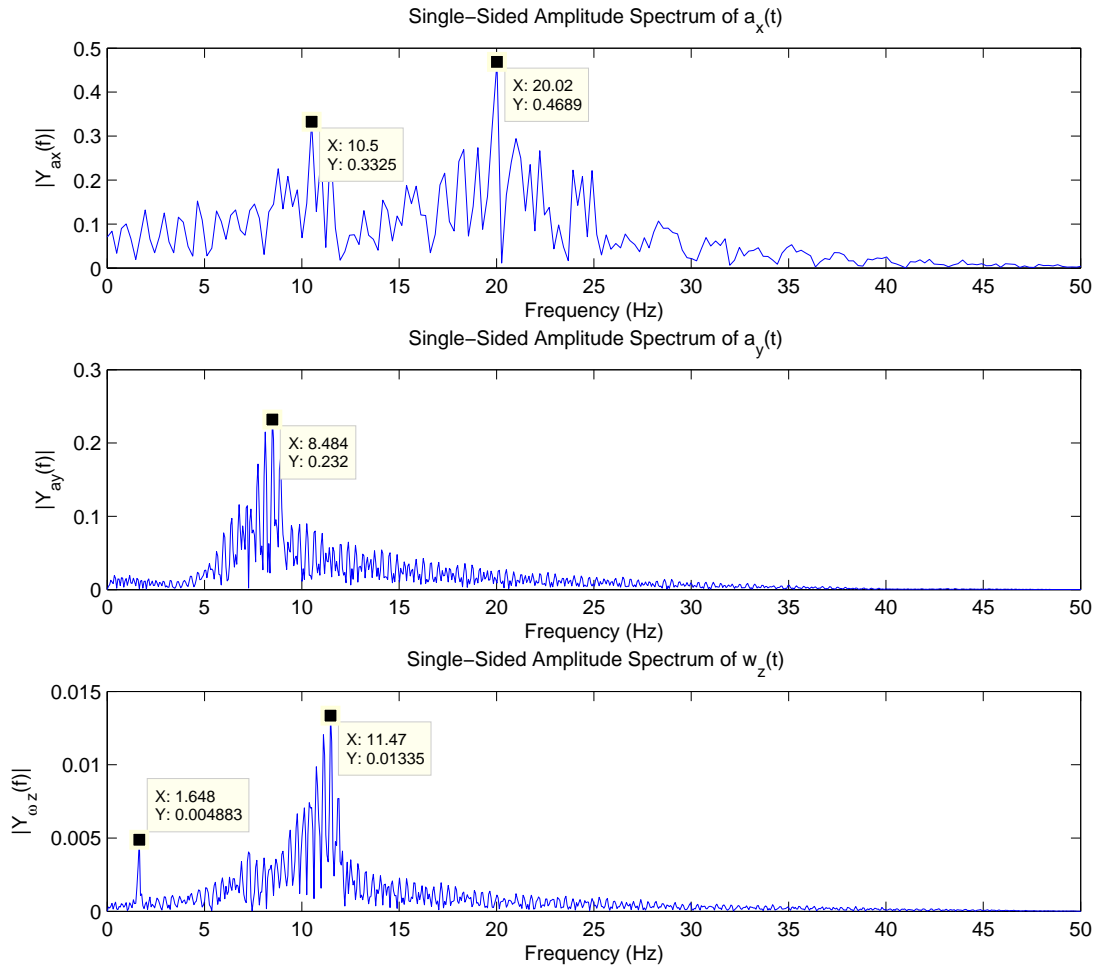
Figure 2.5: Spectral density plots of the acceleration in x, y and θ direction

2.3 Forced vibration analysis

The pendula attached to the MP, shown in Figure 2.1, can be used to periodically excite the system in a desired range of frequencies. An excitation in y-direction can be applied by giving both pendula an offset of 90° and then rotate them in a small angle in phase. An excitation in θ-direction can be achieved by doing the same motion, except now 180° out of phase. An excitation is x-direction is not possible using the pendulums. However, since the the x DOF has clearly the highest eigenfrequency and is therefore most stiff, its the least important DOF to properly control.

By using the pendula to excite the system in a range of different frequencies, a transfer function plot

between the pendulum motor torque and the y-acceleration can be made. This transfer function has been chosen because these values can easily be measured. Although motor torque does not provide any direct insight about the vertical force applied it can still be used to identify the eigenfrequency. Only the magnitude values would change if the exact vertical force would be calculated. The Bode plot in y-direction at position (x,y)=(0,0) is shown in Figure 2.6.
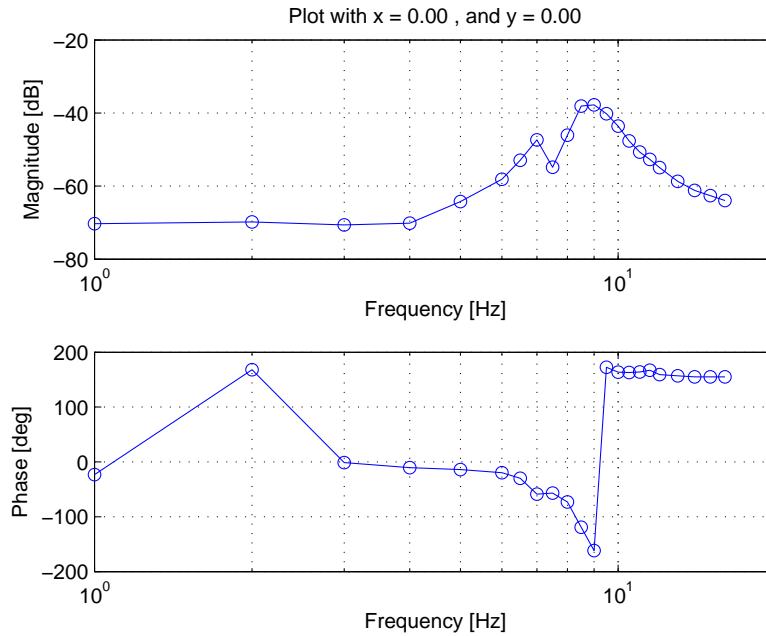

Figure 2.6: Transfer function between the pendulum motor torque and the y-acceleration at position (x,y)=(0,0)

This plot clearly shows a resonance peak at the eigenfrequency of 8.5 Hz, which corresponds to the previous results. However, also a second smaller peak can be observed at a lower frequency of 7 Hz. After experimental validation, it was concluded that this second peak was the result of the natural frequency of the cable tensioners at the bottom cables. These have a significant mass of about 10% of the total mass and will influence the vibrational behaviour of the system. However since these are not part of the system that needs to be identified, this peak is ignored. Doing this, the system behaves as a typical second order system, with a resonance peak and a phase difference that goes from approximately 0 to -180°. The single unexpected measurement of +180° at a frequency of 2 Hz is due to the fact that the response of the system is nearly 0 at such low frequencies and therefore not much confidence can be put on these measurements. The jump to +180° at higher frequencies is due to phase-wrapping.

This method of identification is fast and gives good insight about the eigenfrequency of the system. Therefore this method has been used to identify this parameter at 9 different positions in the

workspace. The eigenfrequencies found at different points in the workspace for both y and θ direction are given in Figure 2.7. Using the eigenfrequency obtained from the measurements, the stiffness coefficient k_y is determined using $k_y = 2\pi m f_{n,y}^2$, where $f_{n,y}$ is the eigenfrequency in Hz. The stiffness in θ direction is calculated using $k_\theta = 2\pi I f_{n,\theta}$.
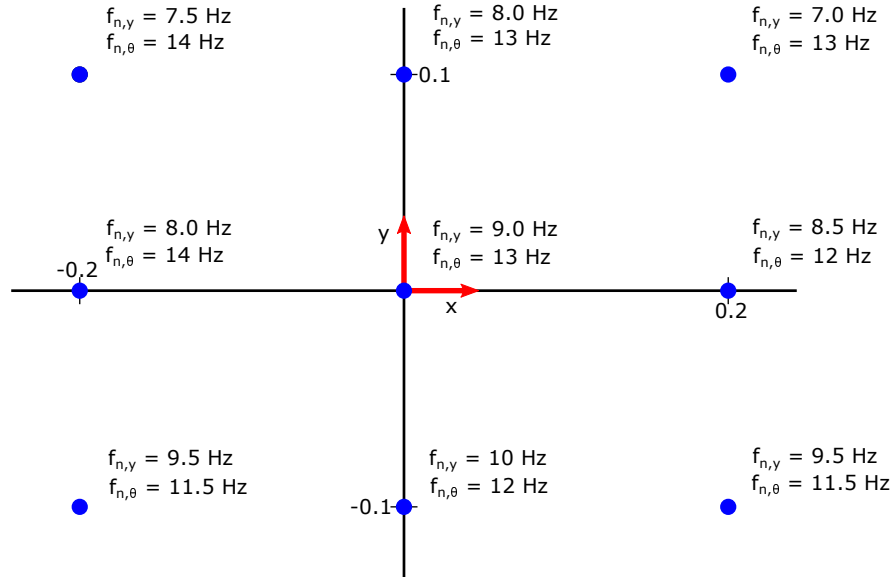

Figure 2.7: The different measured eigenfrequencies in y and θ direction througout the workspace

From Figure 2.7 it can be concluded that the eigenfrequency and therefore the stiffness in y-direction generally increases the lower the MP is positioned. This can explained because the overall stiffness is primarily provided by the upper cables. When the MP is positioned at the top, these upper cables are almost horizontal which means the projection of the upper cable forces in vertical direction is small and can therefore provide little vertical stiffness. If the MP is positioned at the bottom however, the upper cables are more vertical and can therefore provide a higher stiffness in y-direction.

For the θ-direction this trend seems reversed: the stiffness is higher at the top compared to the bottom. The same reasoning as above can be applied, except now the stiffness in x-direction also plays a role, which is largest at the top because of the horizontal orientation of the upper cables.

The difference between the left and right side can be explained due to slight differences in cable lengths and geometry. Also calibration to the (0,0) position is done using a relatively low resolution camera. Therefore it is not guaranteed that the (0,0) position is always the same, which could amount to differences in measurement data.

2.4   Summary of Chapter 2

In this chapter a description of the real system is given. A model is proposed consisting of three decoupled mass-spring-damper components to represent this system. Based on this model the stiffness and vibration characteristics of the system are experimentally identified for 9 different positions of the MP, using various methods.

3 | In-plane vibration control

In this chapter the strategy used for attenuating undesired vibrations during the movement of the MP is described. Two different controllers are proposed: a decoupled PD controller and a LQR controller. The performance of both controllers are evaluated using simulations and the state estimator is described.

The control strategy used to suppress undesired in-plane vibrations during the trajectory is divided in two parts: a trajectory controller and a vibration controller.

The trajectory controller controls the motion of the MP given a certain desired trajectory. For this motion only the upper cables are controlled without feedback and the system is considered to be a rigid body. A schematic view is given in Figure 3.1 where the inputs u_1 and u_2 are the change in length from the initial lengths of the upper cables, δl_1 and δl_2 respectively. The bottom cables both provide an initial tension of around 80 N.
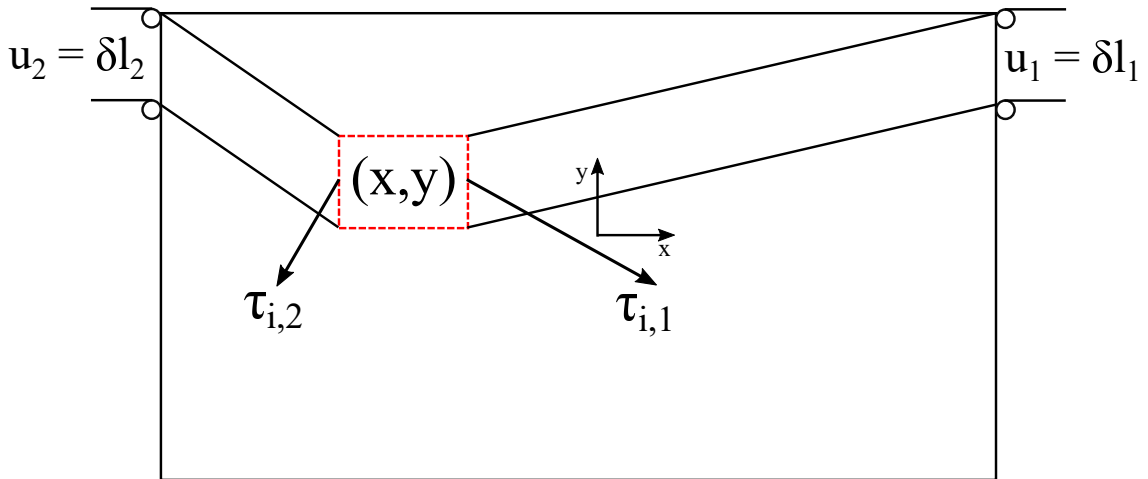

Figure 3.1: A schematic drawing of the rigid body model for moving the MP through the workspace

In reality the system does not behave as a rigid body, since small variations in cable lengths during the movement cause external disturbances on the system. To suppress the in-plane vibrations caused by these disturbances a controller has been created which is superimposed on the rigid body motion. This controller uses the bottom cables as inputs to generate a desired force to counteract the in-plane vibrations. A schematic view of this is given in Figure 3.2. A schematic representation

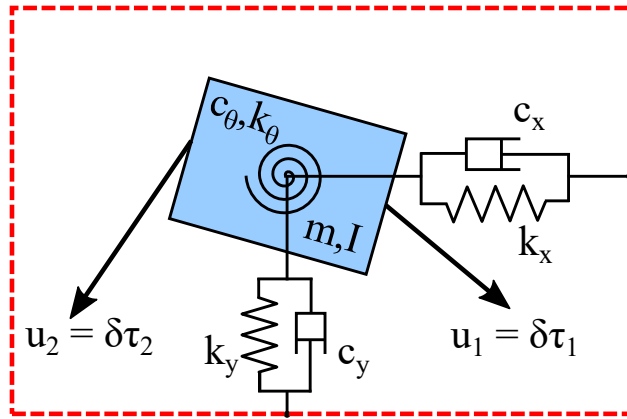of the overall control strategy is shown in Figure 3.3.

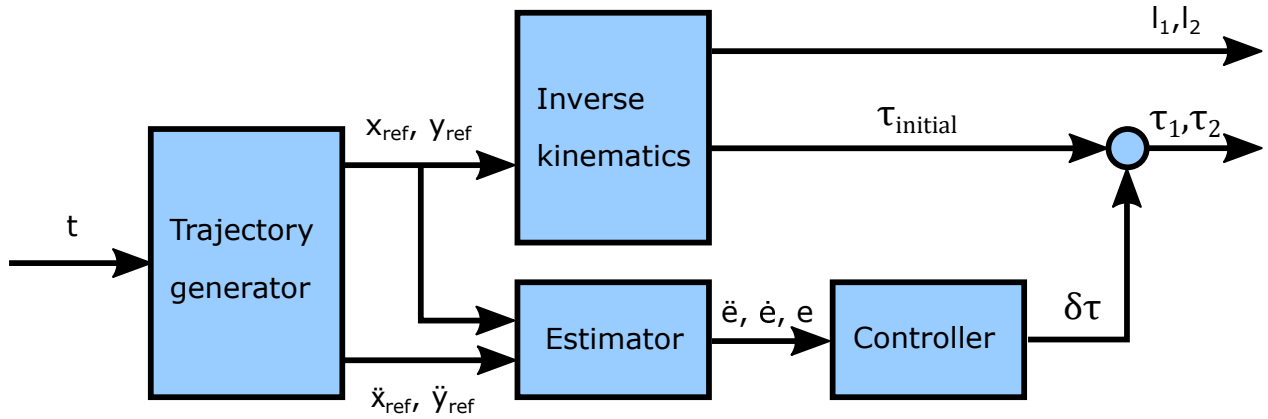Figure 3.2: The vibration model used for vibration control

Figure 3.3: Schematic overview of the control strategy

3.1 Decoupled PD control

The first controller considered is a decoupled PD controller. A PD controller is a feedback controller which uses the error between a desired setpoint and a measured value to adjust the input values. By defining the input as three decoupled forces F_x, F_y and M_z as seen in Figure 3.4, an individual SISO PD controller can be designed for each DOF.
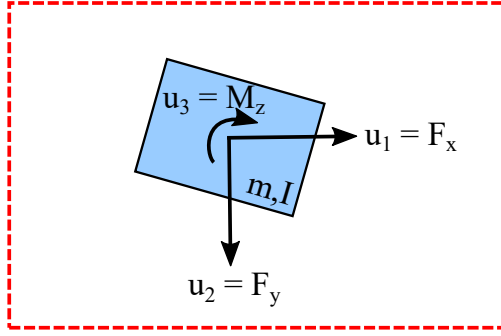
Figure 3.4: Definition of decoupled forces

For this model, the equations of motion can be written as:

$$
M \begin{bmatrix} \ddot{x} \\ \ddot{y} \\ \ddot{\theta} \end{bmatrix} + C(x,y) \begin{bmatrix} \dot{x} \\ \dot{y} \\ \dot{\theta} \end{bmatrix} + K(x,y) \begin{bmatrix} x \\ y \\ \theta \end{bmatrix} = \begin{bmatrix} F_x \\ F_y \\ M_z \end{bmatrix}
$$

Here F_x and F_y are the decoupled input forces in x and y direction respectively and M_z is the moment around the z-axis, as defined in Figure 3.4. x and y are the horizontal and vertical lateral displacements and θ is the rotation of the MP around the z-axis.

To simplify and linearize the model small angles θ are assumed such that the following relations hold: $\cos(\theta) = 1$, $\sin(\theta) = \theta$.

Now the relation between the vector of decoupled input forces $\bar{F}$ and bottom cable tensions τ is given by:

$$
F = \begin{bmatrix} F_x \\ F_y \\ M_z \end{bmatrix} = \underbrace{\begin{bmatrix} \cos(\alpha_1) & -\cos(\alpha_1) \\ -\sin(\alpha_1) & -\sin(\alpha_1) \\ -h\cos(\alpha_1) + w\sin(\alpha_1) & h\cos(\alpha_2) - w\sin(\alpha_2) \end{bmatrix}}_{T} \begin{bmatrix} \tau_1 \\ \tau_2 \end{bmatrix} \tag{3.1}
$$

Here h and w are the vertical and horizontal distances from the center of gravity to the anchor point of the bottom cables respectively and α_1 and α_2 are the angles of the bottom cables and given by:

$$
\alpha_1(x,y) = \arctan(\frac{\frac{b}{2} + y}{\frac{a}{2} - x}), \qquad \alpha_2(x,y) = \arctan(\frac{\frac{b}{2} + y}{\frac{a}{2} + x})
$$

Here x and y gives the position of the MP while a and b are the height and width of the frame suspending the MP respectively. How these parameters are defined is shown in Figure 3.5.

15

When the state X is defined as $X = \begin{bmatrix} x & y & \theta & \dot{x} & \dot{y} & \dot{\theta} \end{bmatrix}^T$ the controlled system can be written in standard control form in the following way:

$$\dot{X} = AX + BF \tag{3.2}$$

The system matrix A is given in Equation 2.4 and control matrix B is defined as:

$$B = \begin{bmatrix} O_{3x3} \\ M^{-1} \end{bmatrix} = \begin{bmatrix} 0 & 0 & 0 \\ 0 & 0 & 0 \\ 0 & 0 & 0 \\ 1/m_p & 0 & 0 \\ 0 & 1/m_p & 0 \\ 0 & 0 & 1/I_z \end{bmatrix} \tag{3.3}$$

where m_p and I_z are defined in Table 2.1.

This would be a controllable system if the inputs were actually the three decoupled forces F. However, ultimately the control input has to be translated to the two cable forces τ_1 and τ_2. Looking at (3.1) reveals a problem, since it is not possible to generate any three decoupled forces using only two inputs so it is not possible to control all three DOF using decoupled PD control. This means that for this underactuated system a choice has to be made between which two DOF will be controlled. Since it was found earlier that the stiffness in y and θ is less than the stiffness in x, these are the two most important DOF to control.

The state space representation for the case where only y and θ are controlled is reduced to:

$$\dot{\bar{X}} = A\bar{X} + B\bar{F}$$

Here $\bar{X} = \begin{bmatrix} y & \theta & \dot{y} & \dot{\theta} \end{bmatrix}^T$, $\bar{F} = \begin{bmatrix} F_y & M_z \end{bmatrix}^T$ and A and B have been reduced appropriately.
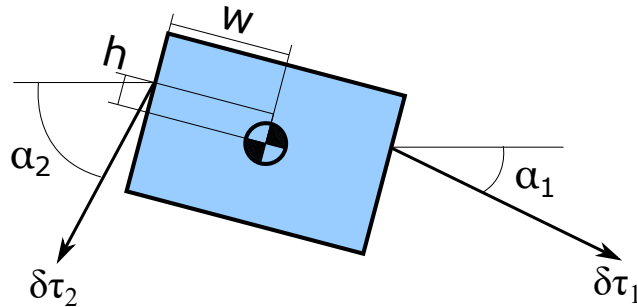

Figure 3.5: Definition of various parameters

Now $\bar{F}$ can be written in terms of bottom cable tensions τ in the following way:

$$\bar{F} = \begin{bmatrix} F_y \\ M_z \end{bmatrix} = \begin{bmatrix} -\sin(\alpha_1) & -\sin(\alpha_2) \\ -h\cos(\alpha_1) + w\sin(\alpha_1) & h\cos(\alpha_2) - w\sin(\alpha_2) \end{bmatrix} \begin{bmatrix} \tau_1 \\ \tau_2 \end{bmatrix}$$
$$= \begin{bmatrix} K_{p,y}\hat{e}_x + K_{d,y}\hat{\dot{e}}_y \\ K_{p,\theta}\hat{e}_\theta + K_{d,\theta}\hat{\dot{e}}_\theta \end{bmatrix} \tag{3.4}$$

Here $\hat{e}_y$ and $\hat{e}_\theta$ indicate the estimates of the position tracking errors. Estimates have to be used since the actual position is not known. How these estimates are obtained is explained in more detail in section 3.3.

With this, the input or required bottom cable tensions can be written as:

$$\bar{u} = \begin{bmatrix} \tau_1 \\ \tau_2 \end{bmatrix} = \begin{bmatrix} -\sin(\alpha_1) & -\sin(\alpha_2) \\ -h\cos(\alpha_1) + w\sin(\alpha_1) & h\cos(\alpha_2) - w\sin(\alpha_2) \end{bmatrix}^{-1} \begin{bmatrix} F_y \\ M_z \end{bmatrix} \tag{3.5}$$

3.1.1 Simulation decoupled PD

The system has been simulated in MATLAB in order to assess the performance of a decoupled PD controller. In this simulation, the vibration reduction capabilities of the controller at a single point has been investigated. So given a certain position of the MP and a certain initial disturbance in x, y and θ, the performance is determined by the time it takes to get the vibration response in those three DOF to zero. For the open loop vibration response of the system the equivalent stiffness found experimentally in Chapter 2 has been used. Since the stiffness is investigated at only 9 points in the workspace, interpolation of these results is used to find an equivalent stiffness at any point in the considered workspace.

The simulation response at position (x,y) = (0.4, 0.1) and with initial state $X_0 = \begin{bmatrix} x_0 & y_0 & \theta_0 & \dot{x}_0 & \dot{y}_0 & \dot{\theta}_0 \end{bmatrix}^T$, with $x_0 = 0.01$ m, $y_0 = 0.04$ m, $\theta_0 = 0.1$ rad is shown in Figure 3.6. Here an iterative trial-and-error approach have been used to find suitable gains. The gains used in this simulation are shown in Table 3.1.

Table 3.1: PD controller gains used in the simulation

	y	θ
K_p	300	10
K_d	30	2

It can be seen that there is no difference between open and closed loop response in x-direction. This

was expected since only the y- and θ-direction are controlled in this simulation. In y and θ a clear reduction in settling time can be observed.
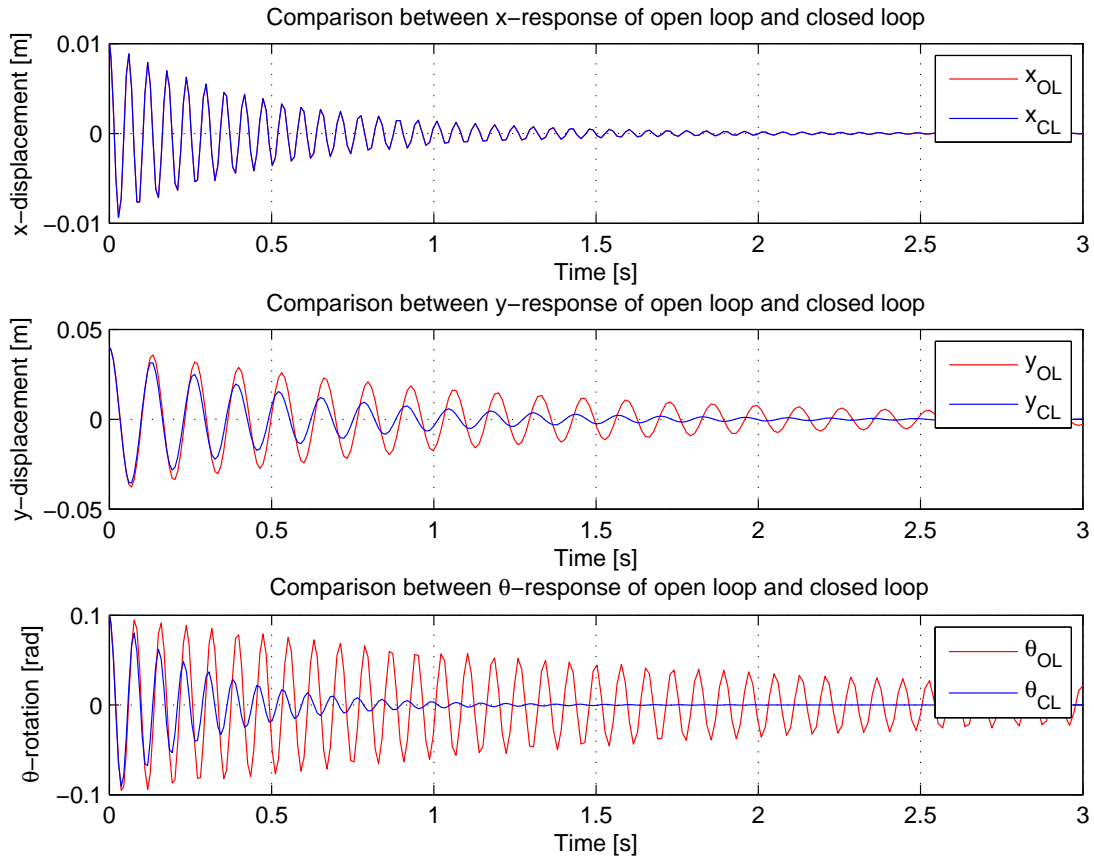

Figure 3.6: Simulation response using the decoupled PD approach at position (x,y) = (0.4, 0.1) and disturbance $[x_0, y_0, \theta_0] = [0.01\ 0.04\ 0.1]$

The control effort is shown in Figure 3.7. This is important to take into account since the cables can only exert a limited unidirectional (positive) force. In this simulation, the bottom cable forces range from 20 to 130 N. Because the platform is not positioned in the middle of the workspace and therefore the orientation of left and right the bottom cable is different, there is a slight difference in tension between the two cables. Apart from this the tensions of the left and right bottom cable show similar behavior.
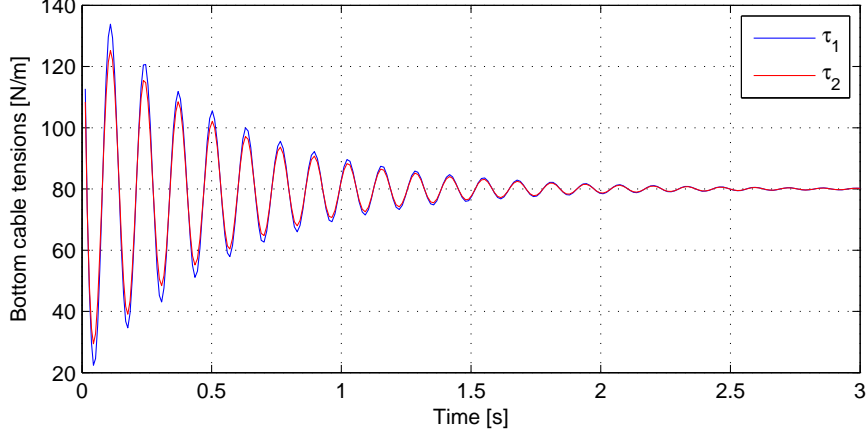
Figure 3.7: Simulated control effort using the decoupled PD approach

3.2 LQR control

The second control strategy considered is using a Linear-Quadratic Regulator (LQR). This is an optimal full state feedback control strategy concerned with minimizing the quadratic cost function given in (3.6) while making a compromise between control effort and performance using two weighting filters Q and R.

$$
\begin{aligned}
\min_{u} \quad & J(u) = \int_0^\infty (X^T Q X + u^T R u) dt \\
\text{s.t.} \quad & \dot{X} = AX + Bu
\end{aligned}
\tag{3.6}
$$

The optimal control law is given by

$$u = -KX$$

Where X is the full state defined in (2.3) and K is defined as:

$$K = R^{-1} B^T P$$

P is found by solving the algebraic Ricatti Equation:

$$A^T P + PA + Q - PBR^{-1}B^T P = 0$$

The main difference between using a LQR approach as opposed to decoupled PD control is that the control forces do not have to be decoupled. This means that instead of defining the control inputs as the three decoupled forces $F = \begin{bmatrix} F_x & F_y & M_z \end{bmatrix}^T$, the two cable tensions τ_1 and τ_2 can be used directly, such that the input becomes: $\bar{F} = \begin{bmatrix} \tau_1 & \tau_2 \end{bmatrix}^T$. This changes the control matrix B in the state-space model given in (3.2) to:

$$B(x,y) = \begin{bmatrix} O_{3x3} \\ M^{-1} \end{bmatrix} T(x,y) \tag{3.7}$$

where the transformation matrix T is defined in (3.1).

Since the optimal cable tensions are determined directly, the restriction of only controlling two DOF disappears. So with an LQR approach it is possible to control all three DOF with only two inputs, while this was not possible when using the decoupled PD approach.

Another difference compared PD control is that a LQR controller requires full state information, whereas PD control only requires the task space tracking errors. This means this control strategy depends on a good state estimator. The state estimator is discussed in more detail in section 3.3.

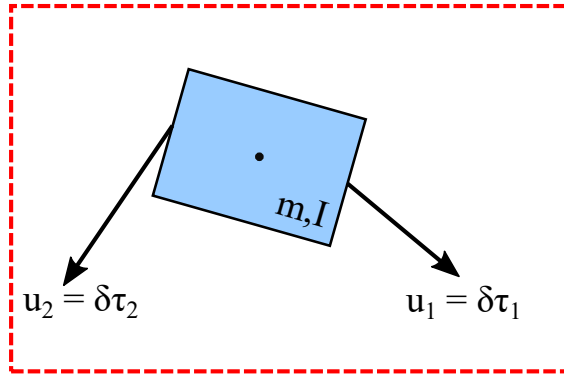The schematic model for this control strategy is given in Figure 3.8.

Figure 3.8: Coupled control used for the LQR approach

3.2.1 Simulation LQR

The system is simulated with similar conditions as the decoupled PD control approach. So at position (x,y) = (0.4, 0.1) and with initial state $X_0 = \begin{bmatrix} x_0 & y_0 & \theta_0 & \dot{x}_0 & \dot{y}_0 & \dot{\theta}_0 \end{bmatrix}^T$, with $x_0 = 0.01$ m, $y_0 = 0.04$ m, $\theta_0 = 0.1$ rad.

The weighting filter Q is determined in an iterative way using educated guesses while weighting filter R is kept as the Identity matrix. For example in the design of Q it has been taken into account that it is more important to control y then it is to control x and the fact that θ is defined in radians instead of meter.

The weighting matrices used in the simulation are:

$$R = \begin{bmatrix} 1 & 0 \\ 0 & 1 \end{bmatrix}$$

$$Q = 4000 \begin{bmatrix} 0.5 & 0 & 0 & 0 & 0 & 0 \\ 0 & 1 & 0 & 0 & 0 & 0 \\ 0 & 0 & .003 & 0 & 0 & 0 \\ 0 & 0 & 0 & 0.5 & 0 & 0 \\ 0 & 0 & 0 & 0 & 1 & 0 \\ 0 & 0 & 0 & 0 & 0 & .003 \end{bmatrix}$$
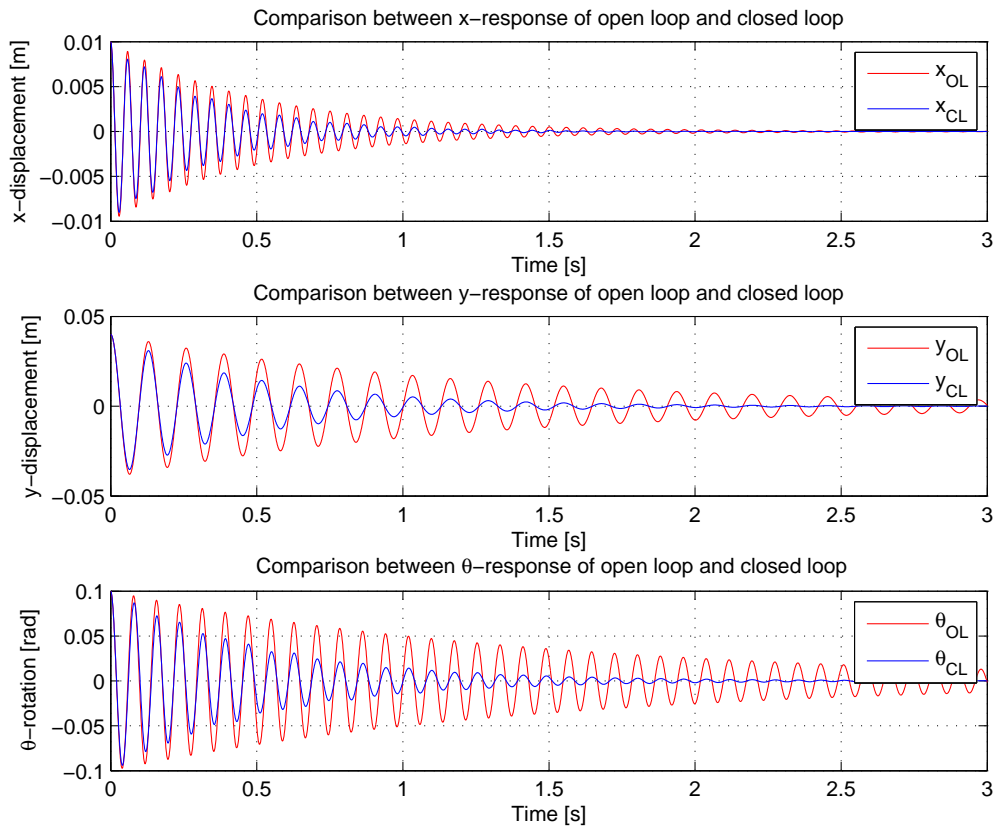

Figure 3.9: Simulation response using the LQR approach at position (x,y) = (0.4, 0.1) and disturbance $[x_0, y_0, \theta_0] = [0.01\ 0.04\ 0.1]$

The open and closed loop simulated vibration response is shown in Figure 3.9. It can be seen from this figure that the vibrations in all three DOF are now damped. With similar values for the

control inputs, shown in Figure 3.10, the overall performance of the controller is comparable to the decoupled PD approach. The control effort shows a bigger difference between left and right cable tensions, since these are controlled much more independently using a LQR approach.
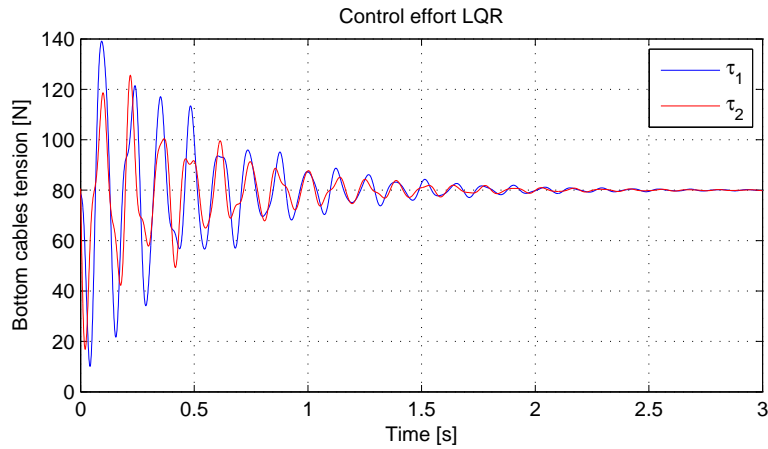

Figure 3.10: Simulated control effort using the LQR approach

3.3 State estimation

The MP is equipped with a 6-axis IMU that can measure three lateral accelerations ($\ddot{x}_m$, $\ddot{y}_m$ and $\ddot{z}_m$) and three rotational velocities ($\dot{\omega}_x$, $\dot{\omega}_y$, $\dot{\omega}_z$). From the trajectory planner the desired accelerations $\ddot{x}$ and $\ddot{y}$ are known. An estimate of acceleration error in x and y direction can be made by subtracting the desired and measured accelerations, which gives:

$$\ddot{e}_x = \ddot{x}_d - \ddot{x}_m$$
$$\ddot{e}_y = \ddot{y}_d - \ddot{y}_m$$

An estimation of the velocity and position error can be obtained by integrating the acceleration error one or twice respectively. However simple integration leads to inaccurate estimates due to inaccuracies of the measurements returned by the IMU as a result of noise and constant bias. The estimates for $\dot{e}$ and e start to drift as a result of these accumulated errors.

To account for the drift the following assumption has to be made: for a large enough window, the moving averages of $\ddot{e}$, $\dot{e}$ and e are zero. This is a valid assumptions since the average of a vibration is zero when a large enough window is considered. This way the estimates can be improved by subtracting the averages from the estimates.

For a good result, the window size has to be a multiple of one period of the vibration. In Figure 3.11 an example of a noisy vibration measurement of 9 Hz is shown. This could represent the vibration

22

in y-direction which has an eigenvalue at approximately 9 Hz. The sample frequency used is 4000 Hz, so by taking a window of $1/9 \cdot 40000$ samples, the average should be zero. For the vibration in θ-direction, this window size is increased to the eigenvalue of the vibration in that direction.

To reduce the noise, a much smaller window has been applied of $1/50 \cdot 4000$ samples to average out the noise.
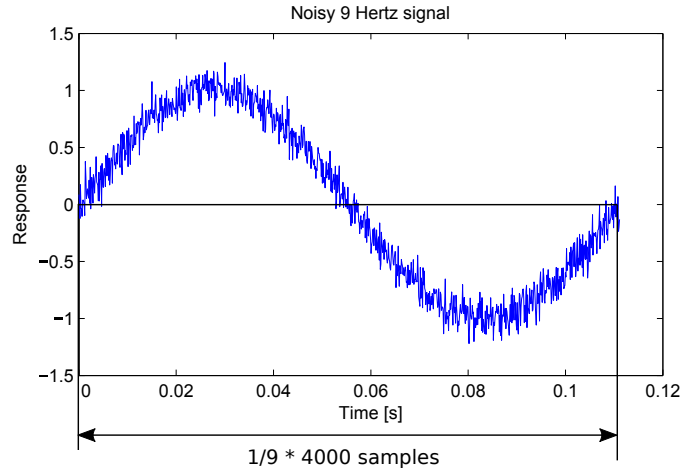

Figure 3.11: Noisy 9 Hz signal

3.4   Chapter 3 summary

The strategy used for controlling the MP is to consider two separate movements: one rigid body movement and one vibrational movement. This way the MP can follow a desired trajectory during which it is considered a rigid body and any undesired vibrations can be attenuated using a controller superimposed on this rigid body movement.

Two controllers are considered to attenuate undesired vibrations: a decoupled PD controller and a LQR controller. The main advantage of using a PD controller is its simplicity while still achieving good performance. However this approach results in an underactuated system, which means that only two out of three DOF can be controlled simultaneously.

Using a LQR approach makes controlling all three DOF using only two inputs possible. The simulated performance is similar to the PD controller, however a LQR controller requires full state feedback. Full state information is not available from the IMU data which means the performance of the controller depends on a good state estimator.

Instead of estimating the full state, the error in terms of acceleration, velocity and position is estimated, since this is the information required by the PD controller.

4 | Experimental results

The performance of the controller has been investigated by comparing the open loop and closed loop y-acceleration and angular velocity.

4.1 PD tuning

The decoupled PD controller has been implemented for the experiments due to its simplicity and good simulation results. However, as is almost always the case, the simulated behaviour does not correspond perfectly to the real system. Therefore the gains found for the PD controller cannot directly be applied to the real system. Instead, an iterative trial-and-error method has been used to find different gains for 9 different positions of the MP where the vibration attenuating is adequate.

The method used for evaluating the performance of a certain combination of gains at a specific position in the workspace is the following. First the robot was brought to the desired position. After that a fast circular trajectory with a small radius of 5 cm was made around that point. During this circular movement the resulting vibrations in the 3 in-plane DOF were recorded and the gains were adjusted such that these vibrations were minimized. This procedure was repeated for all 9 positions in the workspace until different values for the four gains $K_{p,y}$, $K_{d,y}$, $K_{p,\theta}$ and $K_{d,\theta}$ were found depending on the position of the MP. The $K_{p,y}$ gains are shown in Figure 4.1. The other gains are shown in Appendix 2.

The gains at any position in the evaluated workspace can be determined using a cubic interpolation method. This way all four gains change gradually depending on the current position of the MP. An example of how the gains when the robot is given a certain rectangular trajectory change is given in Figure 4.2.

4.2 Performance

The open and closed loop response has been compared for various cases to investigate the performance of the controller. The travelled trajectory remained the same for all cases: a rectangle around the homing position with a width of 0.4 m and a height of 0.2 m. The run time however was varied, one slow and one fast trajectory. To investigate the robustness of the controller a weight of 5.5 kg has been added, increasing the total weight of the MP by 40%.
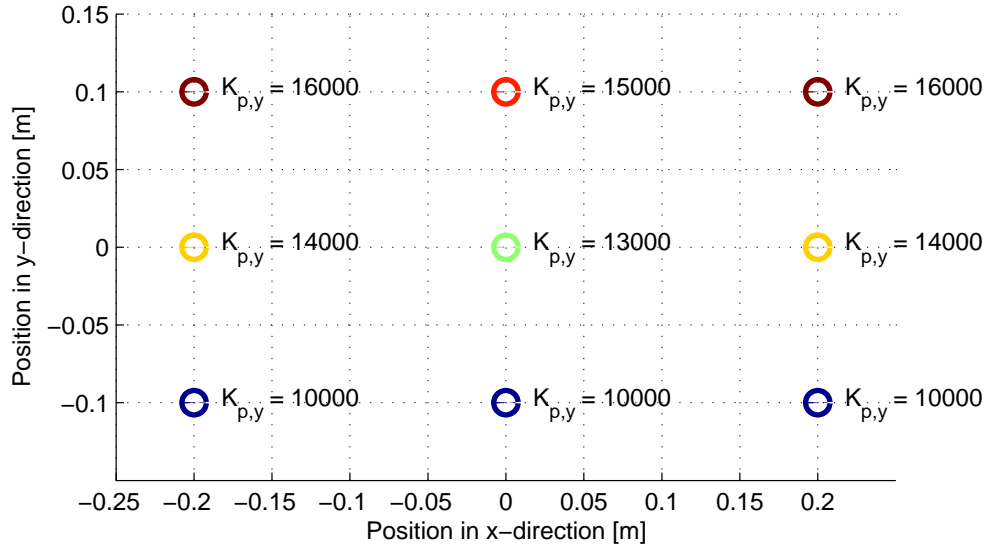
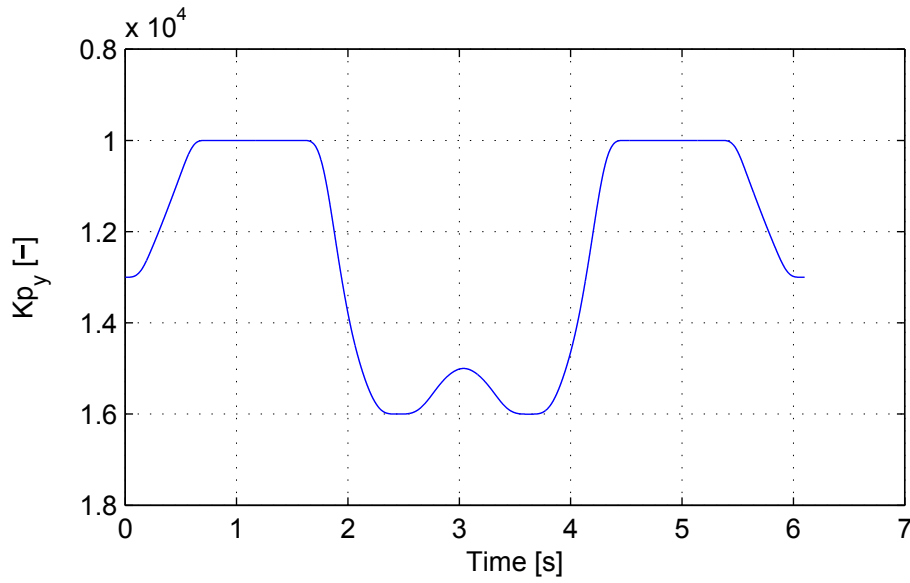Figure 4.1: Experimentally found gains $K_{p,y}$ depending on the position of the MP

Figure 4.2: The gradual change of the gain $K_{p,y}$ during a rectangular movement

25

Case 1: Slow trajectory

The results of the first case are shown in Figure 4.3. In this case the total run time was around 15 seconds and no extra mass was added to the MP.
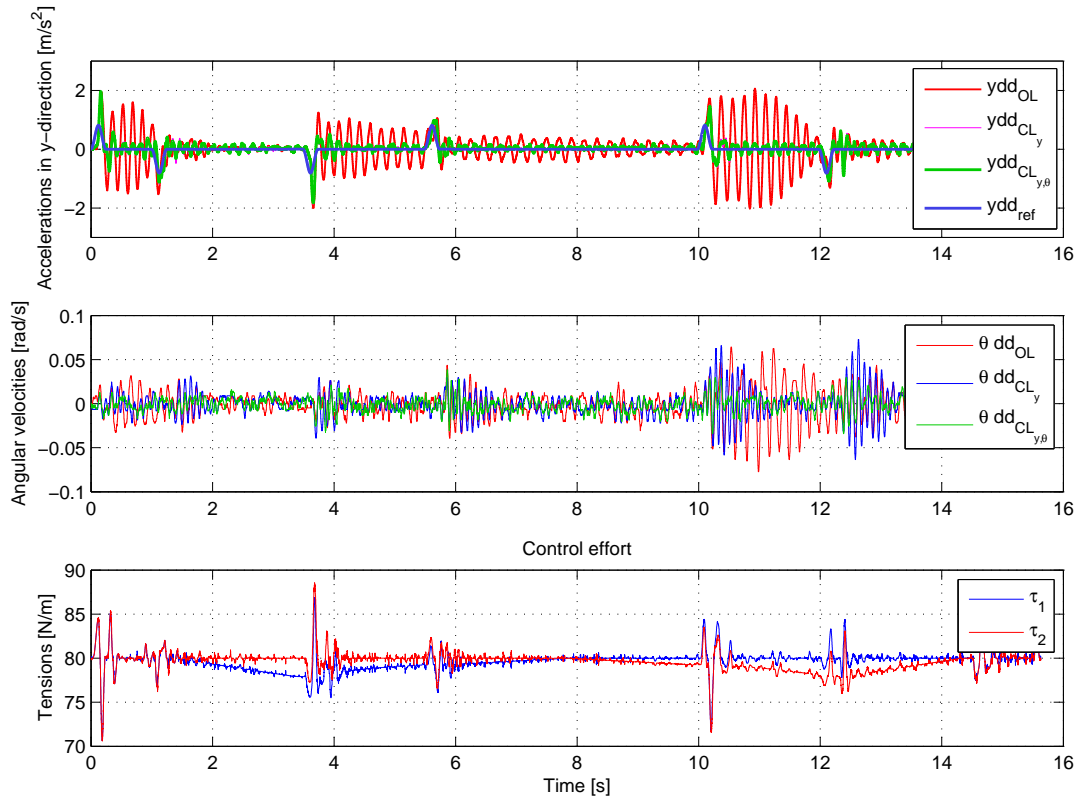

Figure 4.3: Experimental results for a slow rectangular trajectory

In the first plot of Figure 4.3, four lines are plotted. The red line indicates the open loop acceleration in y-direction. The purple line represents the closed loop y-direction when only the vibrations in y-direction are attenuated. The green line shown the performance when both the vibrations in y- and θ-direction are attenuated. Finally the blue line shows the acceleration reference. The second plot shows the open and closed loop angular velocities. The reference is not shown, since this is always zero. The third plot shows the control effort of the bottom cables.

Comparing the open and closed loop performance in y-direction, a clear improvement can be seen. It can also be observed that controlling both y and θ achieves the best overall results. The control effort stays within a range of about 10 N from the initial tension, which is well within acceptable bounds.

Case 2: Fast trajectory

Comparing the results between the open and closed loop when the MP is moved much faster produces Figure 4.4. Similar results are obtained as before, with a significant increase in tracking accuracy when the controller is applied. An interesting thing to note in the first plot of Figure 4.4 is the response delay of the closed loop. This delay is due to the fact that an averaging filter is used to increase the accuracy of the estimates. Introducing a filter always results in a response delay. Another thing to note is the control effort which has now significantly increased compared to the slow trajectory. However, these cable forces are still within the limits that can be produced by the bottom cables.
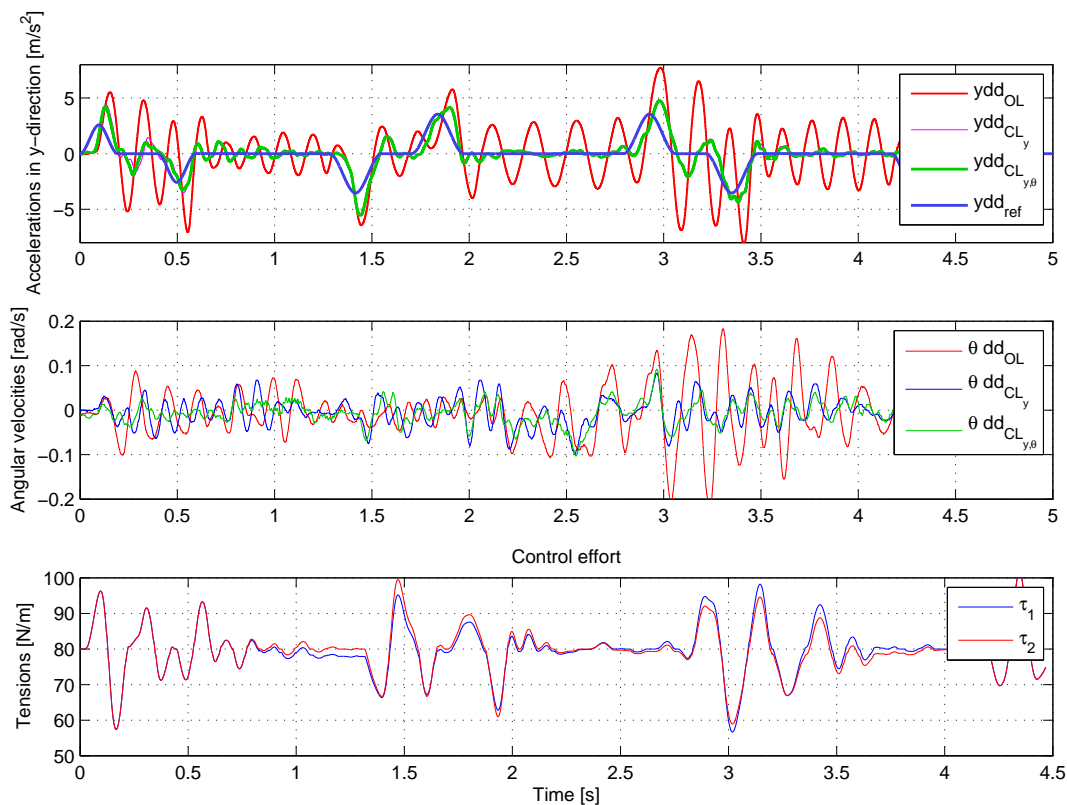

Figure 4.4: Experimental results for a fast rectangular trajectory

Case 3: Slow trajectory with added mass

In order to investigate the robustness of the controller, the mass of the MP has been increased by 40%. This can simulate the scenario of mass being added to the MP as a result of picking up a certain object. The performance of this controller without any changes can be seen in Figure 5.7

in Appendix 5.2. From this figure it can be seen that the open loop seems to be unstable. This was also visually apparent since the vibrations in y-directions became dangerously large. However it can also be seen that closed loop the vibrations are attenuated similarly to the case where no extra mass was added. This indicates that the controller is robust against mass changes and can even stabilize an unstable system.

Case 4: Fast trajectory with added mass

For the last case, a fast trajectory with added mass is investigated and can be seen in Figure 5.5 in Appendix 5.2. These results are similar to the case where no extra mass is added. This confirms the robustness of the controller once again.

4.3   Summary of the results

The experimental results obtained in the previous sections can be evaluated in terms of a standard deviation. This way a quantified value can be assigned to the tracking errors for an easier comparison. The standard deviations for both the vertical y-accelerations and the angular velocities for the four cases described above are given in Tables 4.1 to 4.4. Here OL indicates the open loop, CL_y indicates the closed loop where only the y-direction is controlled and $CL_{y,\theta}$ indicates the closed loop where both the $y/$ and θ-direction is controlled.

Table 4.1: Case 1: slow rectangular trajectory

Standard deviation	OL	CL_y	$CL_{y,\theta}$
vertical acceleration	0.565	0.200	0.203
angular velocity	0.0166	0.0138	0.0083

Table 4.2: Case 2: fast rectangular trajectory

Standard deviation	OL	CL_y	$CL_{y,\theta}$
vertical acceleration	2.612	0.912	0.900
angular velocity	0.0618	0.0311	0.0245

Table 4.3: Case 3: slow rectangular trajectory with added mass

Standard deviation	OL	$CL_{y,\theta}$
vertical acceleration	2.362	0.236
angular velocity	0.0478	0.0199

Table 4.4: Case 4: fast rectangular trajectory with added mass

Standard deviation	OL	$CL_{y,\theta}$
vertical acceleration	1.9377	0.8263
angular velocity	0.0577	0.0303

5 | Conclusions and future work

5.1 Conclusions

Cable driven parallel robots have a great potential in applications where high accelerations and low costs are required. However due to the low stiffness characteristic of cable robots, vibrations tend to occur that quickly limits the performance. Therefore, in order to make cable driven parallel robots a viable application in industry, an active vibration controller is required.

The main goal of this research was to investigate whether it is possible to design an effective in-plane vibration controller based on a simple 3 DOF model with experimentally obtained equivalent stiffness and damping values. Such a simplification would make the need for a complex model obsolete, which could significantly reduce the modeling time.

Various methods have been used to identify the stiffness and eigenvalues of the manipulator in the three in-plane degrees of freedom x, y and θ. This way, a grid has been made which describes the system in these terms across a 2D workspace.

Using these experimentally obtained values, a decoupled PD controller has been designed to attenuate undesired vibrations in y and θ directions. This controller takes the position of the MP in the workspace into account and adjusts the gains accordingly.

Due to imperfect state information, a state estimator has been used to determine the velocity and position of the MP from acceleration data obtained by the body-fixed IMU.

The designed vibration controller has been implemented on a real setup. Experimental data shows a clear attenuation of undesired vibrations in y- and θ-direction by exerting a reasonably small force using the bottom cables. Vibrations in x-direction are not attenuated by the proposed controller. However, vibrations in x-direction are significantly smaller compared to the vibrations in y- and θ-direction, so this limitation of the controller does not limit the overall system performance.

Approximately a factor 2 decrease in vibrations in θ-direction have been obtained. In y-direction, these improvements range from a factor 3 to a factor 10 depending on the test case. It has been shown that the vibration controller can even stabilize an unstable open-loop system.

5.2   Future work

The proposed decoupled PD controller is limited to controlling two DOF only. For controlling all three in-plane DOF several options are available.

The first option is to increase the number of actuators for the vibration control and still use a decoupled PD approach. This can be achieved by also including the upper cables in the vibration control strategy. Including both upper cables results in an overactuated system, which requires additional thought.

It is possible to control all three DOF with only two actuators, as has been shown in simulation. However by doing so the simple decoupled PD approach is not viable anymore. Other optimal or sub-optimal control strategies may be applied instead, such as LQR or MPC.

In order to fully validate the proposed control strategy, the controller should be tested on a full-size setup. This way non-linear effects such as cable elongation and the effect of the mass of the cables can be more easily investigated.

Appendix 1: Free vibration equations of motion

The equations of motion of a single DOF free vibrating system can be written as:

$$m\ddot{q} + c\dot{q} + kq = 0 \tag{5.1}$$

$$\ddot{q} + \frac{c}{m}\dot{q} + \frac{k}{m}q = 0 \tag{5.2}$$

By defining $k/m = \omega_n^2$, $c/m = 2\eta\omega_n$, Equation 5.2 can be written as:

$$\ddot{q} + 2\eta\omega_n\dot{q} + \omega_n^2 q = 0 \tag{5.3}$$

The characteristic equation of Equation 5.3 can be written as:

$$s^2 + 2\eta\omega_n s + \omega_n^2 = 0$$

Which has the following roots:

$$s_{1,2} = -\eta\omega_n \pm \omega_n\sqrt{\eta^2 - 1} = -\eta\omega_n \pm i\omega_d$$

So the general solution can be written as:

$$x(t) = c_1 e^{-at} sin(bt + c_2)$$

Here, $a = \eta\omega_n$, $b = \omega_d = \omega_n\sqrt{\eta^2 - 1}$ and c_1 and c_2 are constants which depend on the initial conditions.

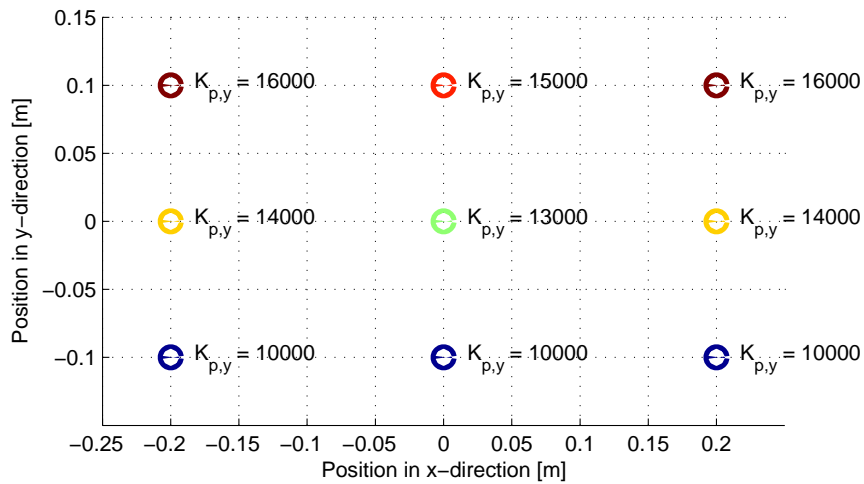# Appendix 2: Experimentally found gains

Figure 5.1: Experimentally found gains $K_{p,y}$ depending on the position of the MP
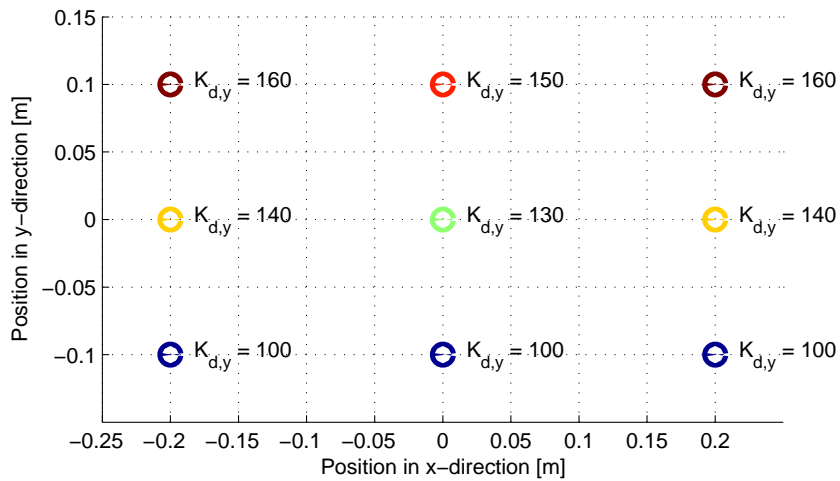

Figure 5.2: Experimentally found gains $K_{d,y}$ depending on the position of the MP
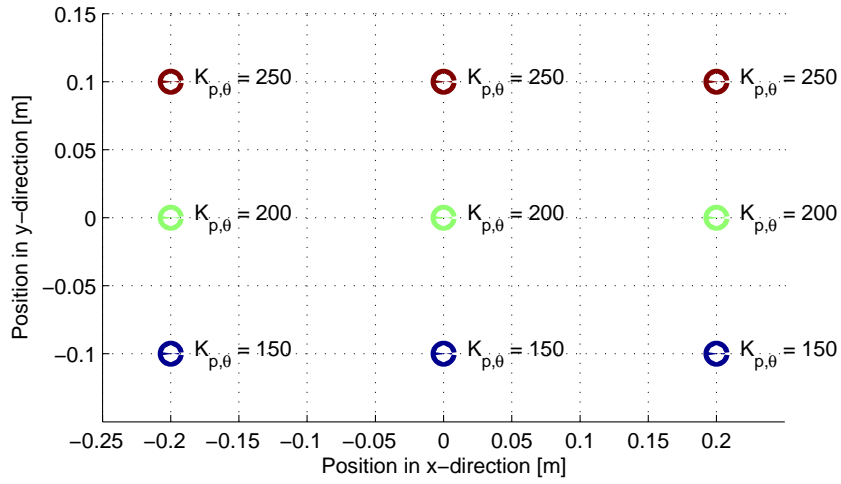
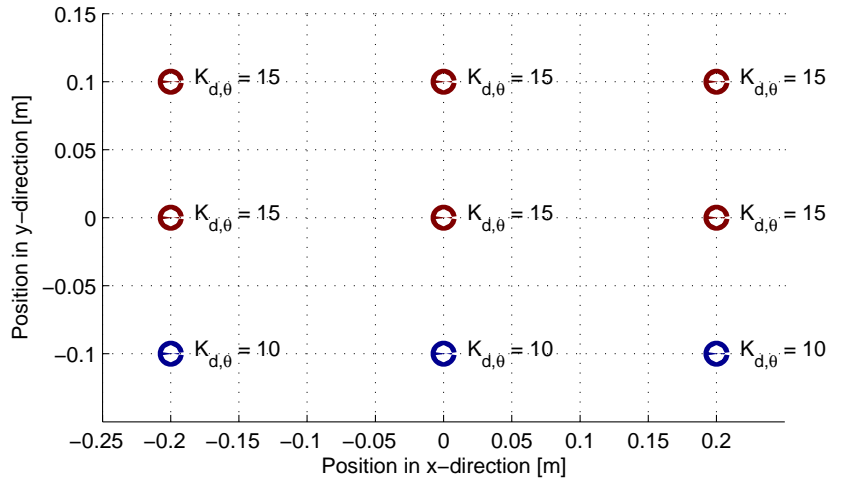Figure 5.3: Experimentally found gains $K_{p,\theta}$ depending on the position of the MP

Figure 5.4: Experimentally found gains $K_{d,\theta}$ depending on the position of the MP
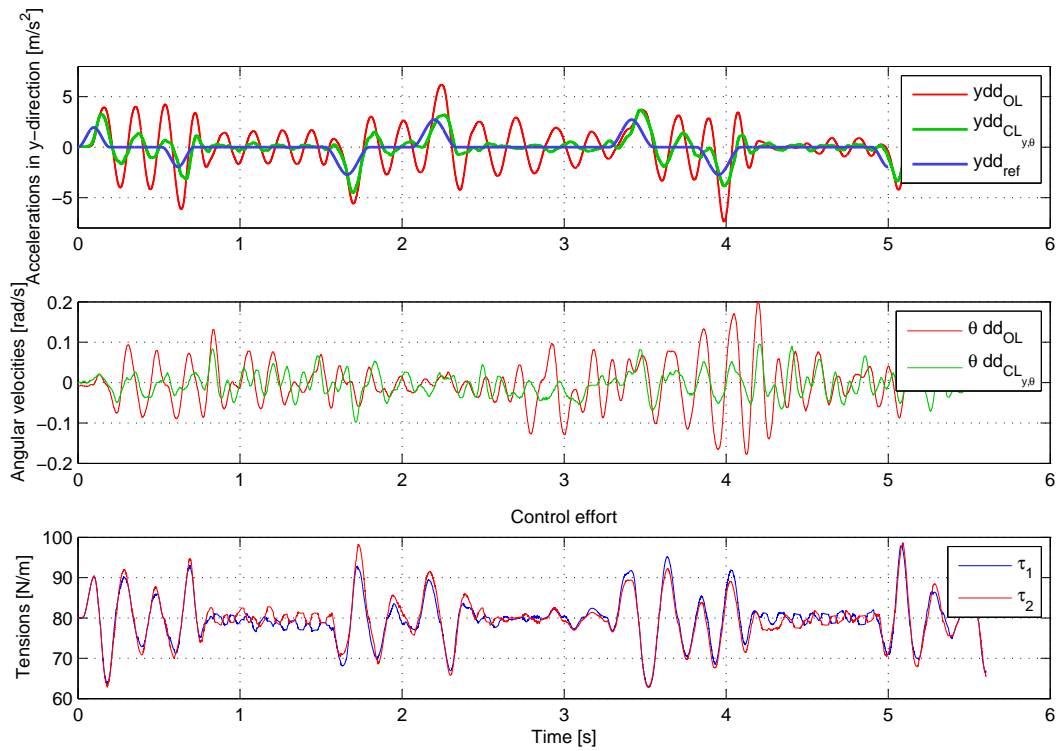
Appendix 3: Experimental results

Figure 5.5: Comparison between open and closed loop for a fast rectangular trajectory with added mass
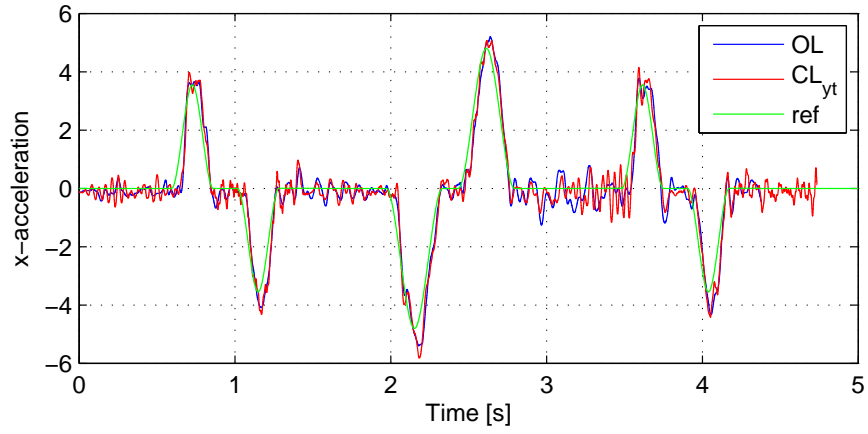
Figure 5.6: Comparison between open and closed loop x-acceleration for a fast rectangular trajectory with no added mass
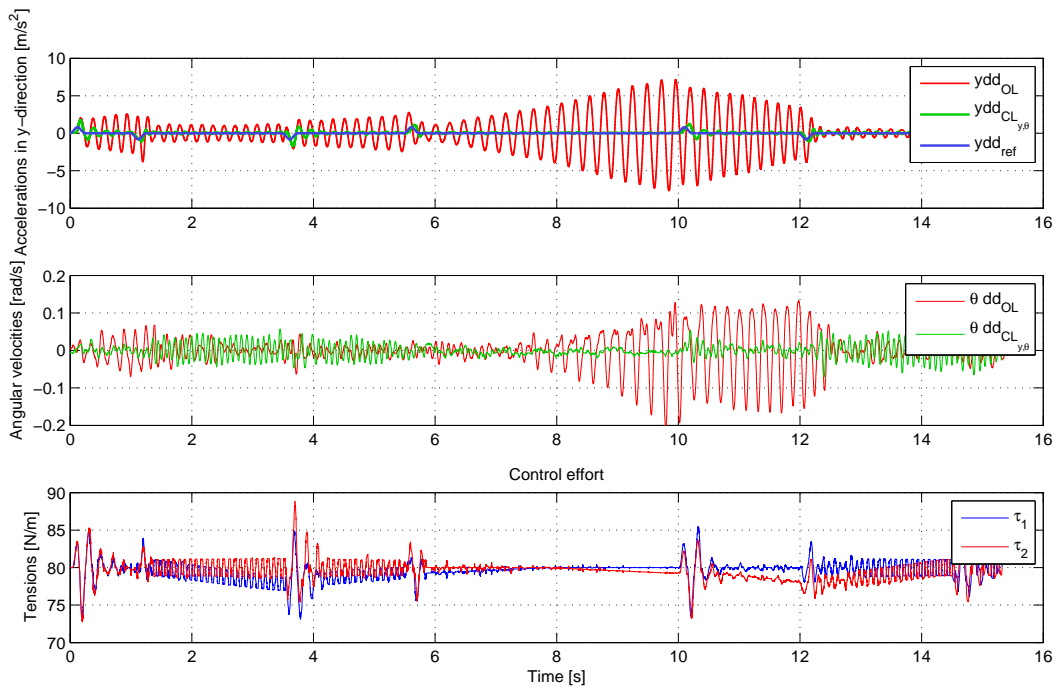

Figure 5.7: Comparison between open and closed loop for a slow rectangular trajectory with added mass

Appendix 4: Matlab code

Create bode plots

```matlab
clear all; close all; clc;

% Load data
data{1} = load('David_Y_SineSweep_x=0_y=0.mat');
data{2} = load('David_Y_SineSweep_x=0_y=0.15.mat');
data{3} = load('David_Y_SineSweep_x=0.4_y=0.15.mat');
data{4} = load('David_Y_SineSweep_x=0.4_y=0.0.mat');
data{5} = load('David_Y_SineSweep_x=0.4_y=-0.15.mat');
data{6} = load('David_Y_SineSweep_x=0_y=-0.15.mat');
data{7} = load('David_Y_SineSweep_x=-0.4_y=-0.15.mat');
data{8} = load('David_Y_SineSweep_x=-0.4_y=0.0.mat');
data{9} = load('David_Y_SineSweep_x=-0.4_y=0.15.mat');

opts = bodeoptions('cstprefs');
opts.FreqUnits = 'Hz';

for j = 1:9
%number of samples to remove from the end
n = 0;

t = data{j}.data(2,12000:end-n)-data{j}.data(2,12000);          %sample 12000 = first 3 seconds of swingup time
y_y = data{j}.data(14,12000:end-n)-mean(data{j}.data(14,12000:end-n));  %acceleration in y direction
u_1 = data{j}.data(25,12000:end-n);
u_2 = data{j}.data(26,12000:end-n);

Freq = [1 2 3 4 5 6 6.5 7 7.5 8 8.5 9 9.5 10 10.5 11 11.5 12 13 14 15 16];

% Cut measurements in 23 parts
sss = floor(length(y_y)/(length(Freq)+1));

u = u_1 + u_2;

% Create data for 22 individual frequencies
clear y_ys u_s

% Define input y_ys and output u_s data
for i = 1:22
    y_ys(i,:) = y_y(1+(i-1)*sss+8600:i*sss);
    u_s(i,:) = u(1+(i-1)*sss+8600:i*sss);
end

% Calculate magnitude and phase difference
for i = 1:22
    mag(i) = abs(y_ys(i,:))/abs(u_s(i,:));
    PhDiff(i) = phdiffmeasure(u_s(i,:), y_ys(i,:));
end

PhDiff = radtodeg(PhDiff);
PhDiff = wrapTo180(PhDiff);
magdb = 20*log10(mag);

% For the plot titles
xx = [0 0 0.4 0.4 0.4 0 -0.4 -0.4 -0.4];
yy = [0 0.15 0.15 0 -0.15 -0.15 -0.15 0 0.15];
str = sprintf('Plot with x = %.2f , and y = %.2f',xx(j),yy(j));
```

```
56
57  figure(j)
58  subplot(2,1,1)
59  semilogx(Freq,magdb,'o-')
60  xlim([1 20])
61  xlabel('Frequency [Hz]')
62  ylabel('Magnitude [dB]')
63  xlim([1 20])
64  grid on
65  title(str)
66  subplot(2,1,2)
67  semilogx(Freq,PhDiff,'o-');
68  xlim([1 20])
69  xlabel('Frequency [Hz]')
70  ylabel('Phase [deg]')
71  grid on
72
73  [~,index] = max(magdb);
74  Eigenfreq(j) = Freq(index);
75  end
```

Curve fitting

```
1   clear all; close all; clc;
2   options.MaxFunEvals = 800;
3   options.TolFun = 1e-6;
4
5   %Load data
6   load('HammerTest_Ay_12-14-15-56.mat')
7
8   %Plot the raw measurement data
9   figure
10  plot(data(2,:),data(14,:)-mean(data(14,:)))
11  grid on
12  title('measurement ay')
13
14  ty = data(2,32580:35548)-data(2,32580);
15  ay = data(14,32580:35548)-mean(data(14,32580:35548));
16
17  %Least square curve fit
18  out_y_predicted = @(a_y,t)  a_y(3).*exp(-a_y(1)*t).*sin(a_y(2)*t+a_y(4))    +    a_y(7).*exp(-a_y(5)*t).*sin(a_y(6)*t+a_y
        (8))
19  a_y0 = [0; 50; 1; 1; 0;50; 1; 1];
20  [ahat_y] = lsqcurvefit(out_y_predicted,a_y0,ty,ay,[],[],options);
21
22  m = 13.7;
23  I = 0.163;
24
25  %Calculate eigenfrequency, stiffness and damping
26  wn1 = sqrt(ahat_y(1)^2+ahat_y(2)^2);
27  fn1y = wn1/(2*pi);
28  k_y1 = (ahat_y(1)^2+ahat_y(2)^2)*m;
29  c_y1 = 2*ahat_y(1)*m;
30
31  wn2 = sqrt(ahat_y(5)^2+ahat_y(6)^2);
32  fn2y = wn2/(2*pi);
33  k_y2 = (ahat_y(5)^2+ahat_y(6)^2)*m;
34  c_y2 = 2*ahat_y(5)*m;
35
36  k_y = min(k_y1,k_y2)
37  c_y = min(c_y1,c_y2)
38
39  figure(2)
40  plot(ty,ay);
41  hold on
42  plot(ty,out_y_predicted(ahat_y,ty),'r')
43  grid on
```

```matlab
44  ylabel('a_y [m/s^2]')
45  xlim([0 0.7])
46  str=sprintf('Acceleration y-direction, f_{n,1} = %.1d, f_{n,2} = %.1d', fn1y, fn2y);
47  title(str)
48  xlabel('Time [s]')
49  legend('Measured y-acceleration','2nd order model fit')
50
51  save('k_y.mat','k_y');
52  save('c_y.mat','c_y');
```

Bibliography

[1] X. Tang, "An overview of the development for cable-driven parallel manipulators," in *Advances in Mechanical Engineering*, February 2014.

[2] C. Gosselin, "Cable-driven parallel mechanisms: state of the art and perspectives," in *Mechanical Engineering Reviews*, 2014.

[3] R. Dekker, A. Khajepour, and S. Behzadipour, "Design and testing of an ultra-high-speed cable robot," in *International Journal of Robotics and Automation*, 2006.

[4] S. Kawamura, W. Choe, S. Tanaka, and S. R. Pandian, "Development of an ultrahigh speed robot falcon using wire drive system," in *Robots and Automation*, vol. 1, pp. 215–220, 1995.

[5] D. R. Altschuler, "The national astronomy and ionosphere center's (naic) arecibo observatory in peurto rico," in *Single-Dish Radio Astronomy: Techniques and Applications*, vol. 278, 2002.

[6] M. A. Khosravi and H. D. Taghirad, "Robust pid control of fully-constrained cable driven parallel robots," in *Mechatronics*, 2014.

[7] R. L. Williams and P. Gallina, "Translational planar cable-direct-driven robots," in *Journal of Intelligent and Robotic Systems*, 2003.

[8] M. A. Khosravi and H. D. Taghirad, "On the modelling and control of fully constrained cable driven robots with flexible cables," in *Control, Instrumentation and Automation*, 2011.

[9] Y. B. Bedoustani, H. D. Taghirad, and M. M. Aref, "Dynamics analysis of a redundant parallel manipulator driven by elastic cables," in *Control, Automation, Robotics and Vision*, 2008.

[10] M. Rushton, "Vibration control in cable robots using a multi-axis reaction system," 2016.

[11] H. Jamshidifar, "Integrated trajectory and vibration control of a kinematically-constrained warehousing robot," 2015.